Effect of Prior β-Grain Size on the Hot Deformation Behavior of Ti-6Al-4V: Coarse vs Coarser

Y.V.R.K. Prasad, T. Seshacharyulu, S.C. Medeiros, and W.G. Frazier

(Submitted 18 August 1999; in revised form 14 September 1999)

The hot deformation behavior of extra low interstitial (ELI) grade Ti-6Al-4V with a transformed β-preform microstructure was studied in coarse (0.5 to 1 mm) and coarser (2 to 3 mm) (prior β) grained materials using hot compression testing in the temperature range of 750 to 1100 °C and a strain rate range of 0.001 to 100 s^{-1}. Processing maps were developed on the basis of the flow stress data as a function of temperature and strain rate. The maps revealed that the domain of globularization of the lamellar structure and region of large grained superplasticity of β were not influenced by the prior β-grain size. However, the regimes of cracking at the prior β-grain boundaries occurring at lower temperatures and strain rates and the flow instability occurring at lower temperatures and higher strain rates were both wider for the coarse grained material than the coarser grained material. The β- instability regime, however, was more pronounced in the coarser grained material. From the hot workability viewpoint, the present results show that there is no remarkable benefit in refining the prior β-grain size. On the contrary, it will somewhat restrict the workability domain by widening the adjacent regimes, causing microstructural damage.

Keywords grain size, hot processing, titanium, Ti-6Al-4V alloy

1. Introduction

The Ti-6Al-4V is a two-phase titanium alloy with a β transus ($\alpha + \beta \rightarrow \beta$) in the temperature range of 970 to 1020 °C depending on the interstitial impurity (primarily oxygen) content. The alloy is extensively used in the aerospace industry, and the extra low interstitial (ELI) grade is preferred for applications where high fracture toughness is an important requirement.[1] The primary processing of Ti-6Al-4V ingots generally involves hot working in the β range, air cooling to obtain a transformed β microstructure, and mechanical working in the α-β range to obtain fine grained equiaxed ($\alpha + \beta$) structure. Such a microstructure results in good fracture toughness and low cycle fatigue properties. Conversely, the transformed β microstructure consists of acicular or lamellar morphology depending on the rate of cooling from the β-solutionizing temperature, and this type of microstructure results in good creep resistance and high temperature strength. Air cooling, for example, produces Widmanstätten colonies of ($\alpha + \beta$) lamellae within large prior β grains with their boundaries containing a thin primary α layer. The prior β-grain size has an influence on the mechanical properties, and sizes below about 200 μm are considered desirable.[2] In view of faster diffusion rates, hot working in the β range produces very coarse prior β grains, and refinement by β recrystallization often requires interspacing the β forging with a few steps of α-β forging. While a finer prior β-grain size is beneficial for the mechanical properties in the heat-treated component, its influence on the hot workability in the α-β regime is not clearly understood. Semiatin *et al.*[3] reported that the reduction in hot ductility with a decrease in temperature is greater for larger prior β-grain sizes, and the ductility trough is deeper. Suzuki *et al.*[4] explained such an effect in terms of void formation and growth occurring during sliding at the thin β layer in between the primary alpha and the Widmanstätten sideplates. While the prior β-grain size is expected to have an effect on the fracture processes occurring at the prior β-grain boundaries, it is important to understand its influence on all the mechanisms that influence hot workability. The goal of this study was to examine the effect of prior β-grain size on the overall hot working behavior of Ti-6Al-4V with a transformed β-starting (Widmanstätten) microstructure. For this purpose, studies were conducted on coarse vs coarser prior β structures of an ELI grade Ti-6Al-4V.

In this study, the approach of processing maps was adopted to represent and analyze the constitutive behavior of Ti-6Al-4V during hot deformation. The basis and principles of this approach have been described elsewhere,[5,6] and its application to the hot working of a wide range of materials has been compiled recently.[7] In brief, depicted in a frame of temperature and strain rate, power dissipation maps represent the pattern in which power is dissipated by the material through microstructural changes. The rate of this change is given by a dimensionless parameter called the efficiency of power dissipation:

$$\eta = \frac{2m}{m+1} \qquad \text{(Eq 1)}$$

where m is the strain rate sensitivity of flow stress. Over this frame is superimposed a continuum instability criterion for identifying the regimes of flow instabilities, developed on the basis of extremum principles of irreversible thermodynamics as applied to large plastic flow[8] and given by another dimensionless parameter:

$$\xi(\dot{\varepsilon}) = \frac{\partial \ln(m/m+1)}{\partial \ln \dot{\varepsilon}} + m \qquad \text{(Eq 2)}$$

where $\dot{\varepsilon}$ is the applied strain rate. Flow instabilities are predicted to occur when $\xi(\dot{\varepsilon})$ is negative. These two maps together consti-

Y.V.R.K. Prasad, T. Seshacharyulu, S.C. Medeiros, and **W.G. Frazier** Materials Process Design Branch, Materials and Manufacturing Directorate, Air Force Research Laboratory, Wright-Patterson Air Force Base, OH 45433.

tute a processing map that exhibits domains with local efficiency maxima representing certain specific microstructural mechanisms together with regimes of flow instabilities.

2. Experimental Procedures

2.1 Materials

The Ti-6Al-4V alloy used in this investigation was of an ELI grade and had the following composition (wt.%): 6.04-Al, 3.91-V, 0.13-O, 0.08-Fe, 0.008-N, with titanium balance. The β transus for this material was about 970 °C. The alloy was upset forged in the β range at 1180 °C, α-β cogged at 960 °C, and β cogged at 1080 °C, followed by water quench. Due to differential deformation history from the surface to the center, different prior β-grain sizes were produced in the cogged billet. The center region of the billet had a prior β-grain size in the range 2 to 3 mm (called "coarser" hereafter), while the surface region had a range of about 0.5 to 1.0 mm (called "coarse" hereafter). Figures 1(a) and (b) show the initial microstructures of these two grain sizes. It can be noted that minor variations in the thickness of the primary α layer at the prior β boundary and in the size of the Widmanstätten colonies also existed in these microstructures.

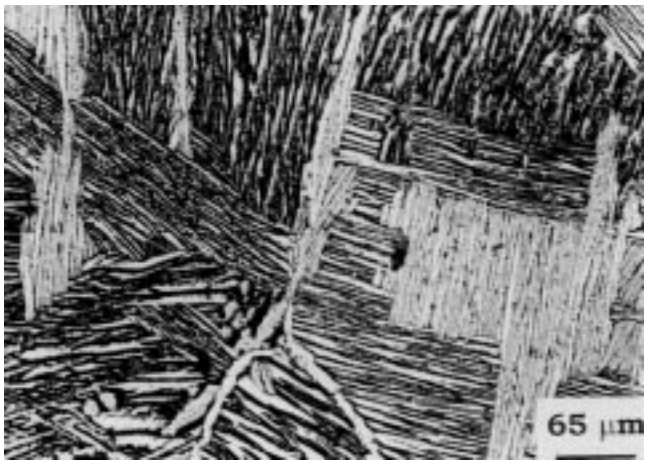

(a)

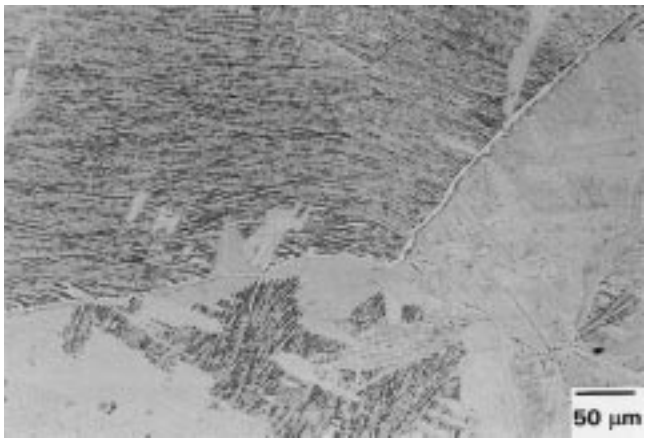

(b)

Fig. 1 Initial microstructures of Ti-6A1-4V used for testing: **(a)** coarser (2 to 3 mm) and **(b)** coarse (0.5 to 1 mm) prior β-grain sized material

2.2 Hot Compression Testing

Isothermal, constant true strain rate compression tests were conducted using a servohydraulic testing machine over the temperature range of 750 to 1100 °C at 50 °C intervals and at constant true strain rates 0.001, 0.01, 0.1, 1, 10, and 100 s^{-1}. Specimens of 15 mm height and 10 mm diameter were used for testing in the α-β range, while larger specimens of 22.5 mm height and 15 mm diameter were used to obtain accurate flow stress measurements in the β range. The specimens were coated with a borosilicate glass paste for lubrication and environmental protection. They were deformed to half the height in each case to impose a true strain of about 0.7 and were air cooled to room temperature after deformation. The deformed specimens were sectioned parallel to the compression axis and prepared for microstructural examination using standard techniques. The specimens were etched with Kroll's reagent, and polarized light micrographs were recorded.

2.3 Flow Stress Data Analysis

The load-stroke data obtained from the compression tests were processed to obtain true stress-true plastic strain curves using the standard method. The data were corrected for adiabatic temperature rise (significant at higher strain rates) using a linear interpolation between ln (σ) and ($1/T$), where σ is flow stress and T is temperature in Kelvin. The strain rate sensitivity, m, was computed using a spline interpolation between ln (σ) and ln ($\dot{\varepsilon}$), and this procedure was repeated at different temperatures. The power dissipation efficiency parameter and instability parameter were calculated as a function of temperature and strain rate at different strains as per Eq 1 and 2, respectively, and were plotted in the temperature-strain rate plane to obtain power dissipation and instability maps.

3. Results and Discussion

3.1 Stress-Strain Behavior

Figures 2 and 3 show the true stress-true plastic strain curves obtained on the coarse and coarser grained Ti-6Al-4V at 800 °C (α-β range) and 1100 °C (β range), respectively. In the α-β range (Fig. 2a and b), the curves exhibited continuous flow softening, which is typically observed in transformed β microstructures.[9] It can be noted that at lower strain rates (<0.1 s^{-1}), the extent of flow softening is not dependent on the prior β-grain size, while at higher strain rates, the flow softening is more prominent in the coarse grained material (Fig. 2b) than in the coarser material. Differences with grain size are also observed in the β-deformation range (Fig. 3a and b). In the coarse grained material (Fig. 3b), steady-state, stress-strain curves were obtained at strain rates below about 1 s^{-1} with similar behavior observed in the coarser material at strain rates below about 0.1 s^{-1}. A significant difference is observed at higher strain rates where the curves exhibited broad oscillations that are more striking and have extended to lower strain rates in the coarser material (Fig. 3a).

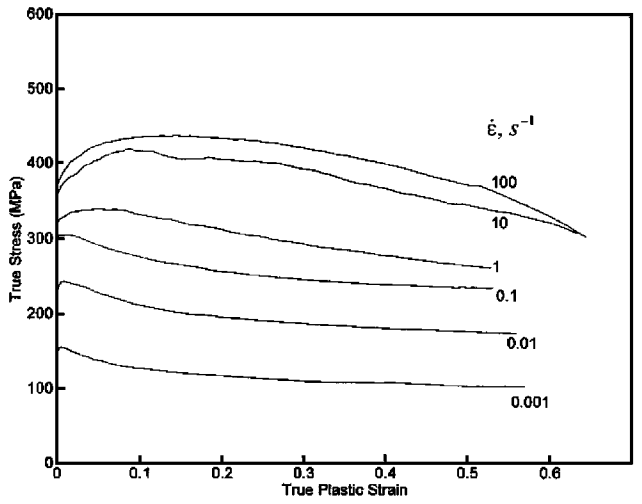

(a)

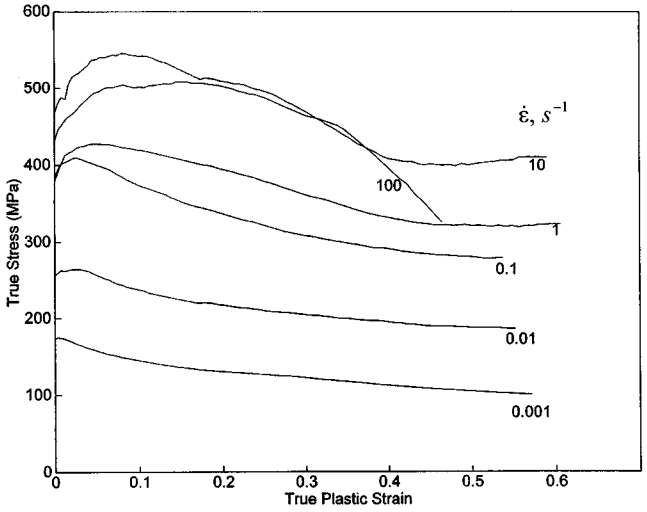

(b)

Fig. 2 Flow curves obtained on Ti-6A1-4V in the α-β regime (800 °C) and different strain rates: **(a)** coarser grained material and **(b)** coarse grained material

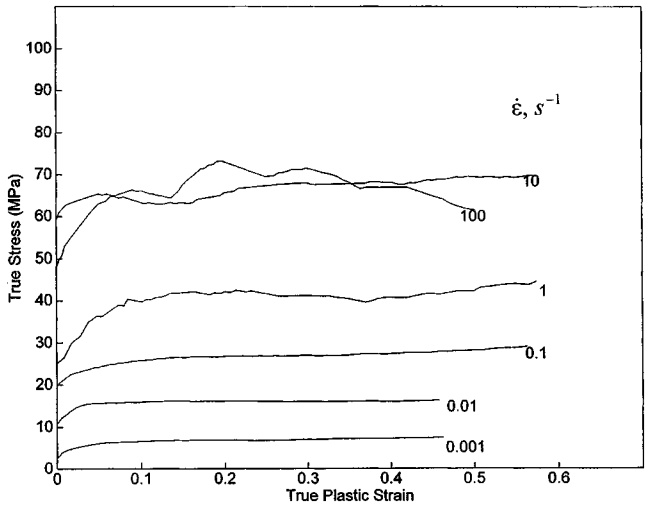

(a)

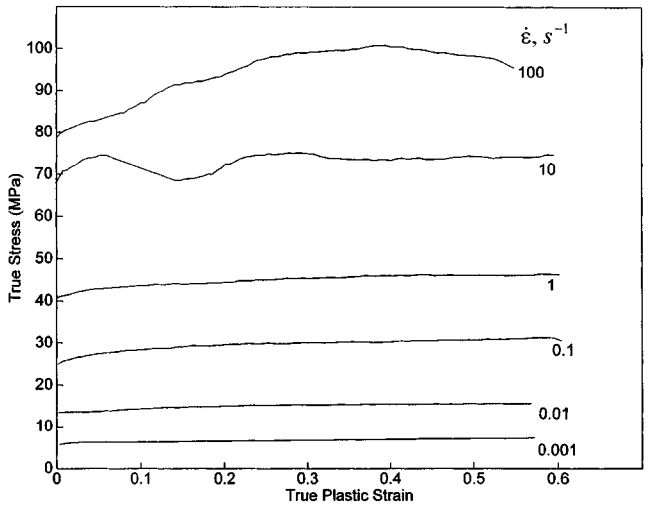

(b)

Fig. 3 Flow curves obtained on Ti-6A1-4V in the β regime (1100 °C) and different strain rates: **(a)** coarser grained material and **(b)** coarse

3.2 Processing Maps

The processing maps obtained on the two grain sizes corresponding to a true plastic strain of 0.5 are shown in Fig. 4(a) and (b). The contour numbers in the map represent the percent of efficiency of power dissipation (Eq 1), and the shaded area represents the regime where flow instability is predicted (Eq 2). The maps obtained at lower strains are not significantly different from those presented in Fig. 4, suggesting that strain within this range does not have a major influence.

The map for the coarser grained material (Fig. 4a) exhibits a single domain at strain rates lower than about 1.0 s^{-1} and over a wide temperature range with a local efficiency maximum of about 46%. The map also reveals two regimes of flow instability—one at temperatures below about 825 °C (α-β range) and strain rates above 0.1 s^{-1} and the other at temperatures higher than about 1050 °C (β range) and strain rates above 10 s^{-1}.

The single domain occurring at lower strain rates covers both the α-β and the β ranges, and therefore, must represent the mechanisms of hot deformation of ($\alpha+\beta$) and β-phase microstructures. In general, the map delineates the temperature of phase transformation by exhibiting points of inflexion (change in the curvature) in the contours around this temperature.[7] In the present case, such inflexions are not clearly evident, and this result is interpreted in terms of merging of domains with similar efficiencies of power dissipation across the transus. At the transus, such a merging has been attributed[10] to the sliding of intercolony boundaries that may cause void nucleation at their triple junctions. Such a process will have an efficiency of power dissipation similar to the adjacent processes and will result in a sharp drop in the tensile ductility.

3.3 Globularization Domain

In the α-β regime, the microstructures recorded on the deformed specimens exhibited globularization of the lamellar microstruc-

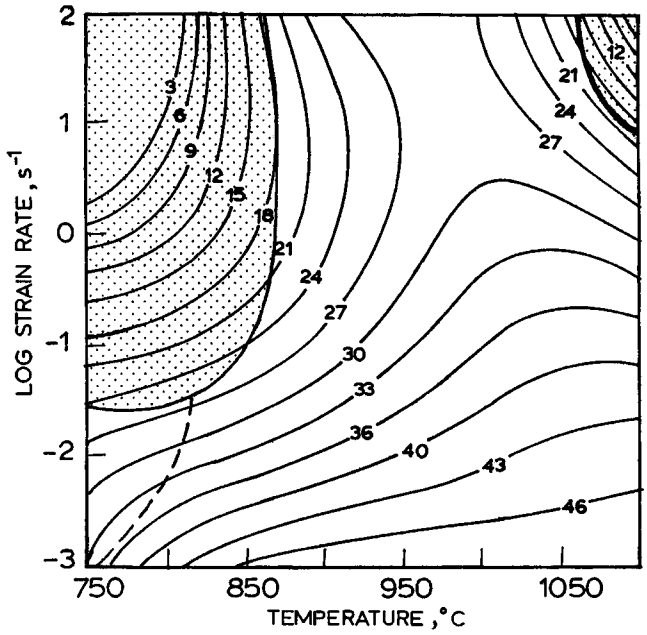

(a)

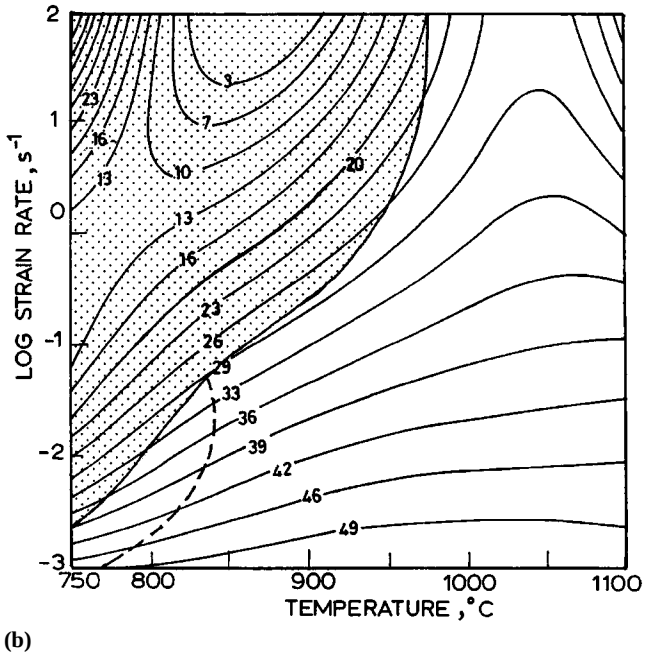

(b)

Fig. 4 Processing maps obtained on Ti-6A1-4V at a true plastic strain of 0.5: **(a)** coarser grained material and **(b)** coarse grained material. Contour numbers represent percent efficiency of power dissipation. Shaded region corresponds to flow instability. Dotted boundary represents the upper limits of prior β-boundary cracking

ture. Figure 5(a) shows a typical specimen, which corresponds to a coarser grained specimen deformed to a true strain of about 0.7 at 900 °C and 0.001 s^{-1}. In this domain, the extents of globularization and the globular size are less at lower temperatures and higher strain rates. The mechanism of globularization has been discussed elsewhere.[10] Briefly, the process consists of shearing of the lamellae, which are favorably oriented to the stress axis; simultaneous occurrence of dynamic recovery by cross-slip to

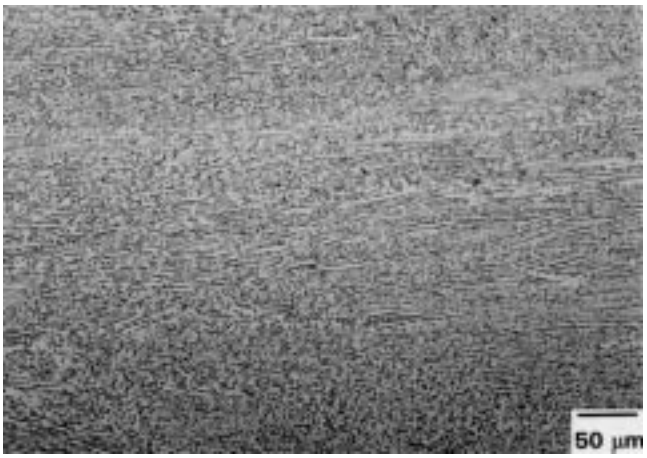

(a)

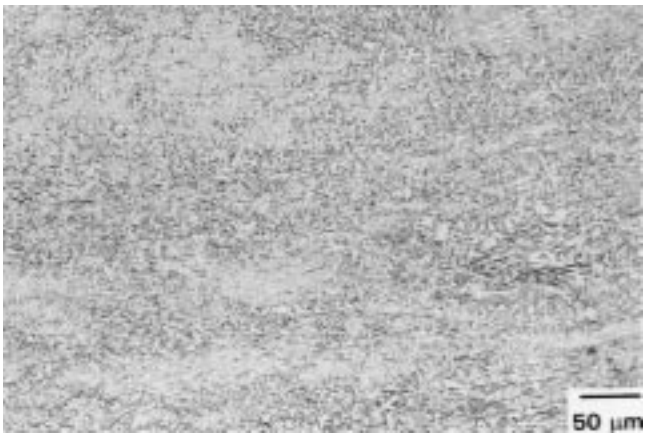

(b)

Fig. 5 Microstructures obtained on Ti-6A1-4V specimens deformed at 900 °C and 0.001 s^{-1} exhibiting globularization of lamellar structure: **(a)** coarser grained material and **(b)** coarse grained material

nucleate an interface; and migration of the interfaces to form globules for reducing the total interface energy. The rate controlling step, however, was evaluated to be the occurrence of the cross-slip.[11] On the basis of the temperature dependence of flow stress, which follows the kinetic rate equation given by

$$\dot{\varepsilon} = A\sigma^n \exp(-Q/RT) \quad \text{(Eq 3)}$$

where $\dot{\varepsilon}$ is the strain rate, A is a constant, σ is the flow stress, n is the stress exponent, Q is the activation energy, R is the gas constant, and T is the temperature, the apparent activation energy for the globularization process has been calculated. Figure 6 shows the Arrhenius plot, demonstrating the variation of flow stress with temperature at a strain rate of 0.001 s^{-1}, which confirms the validity of Eq 3 and shows that the apparent activation energy is approximately 394 kJ/mole for this process.

Figure 4(b) shows the processing map for the coarse grained material, which exhibits two domains. The first domain is at lower strain rates (<0.1 s^{-1}) covering a wide temperature range with a local maximum of efficiency of power dissipation of about 49%. This domain is very similar to the domain described previously for

the coarser grained material (Fig. 4a). The second domain occurs at temperatures lower than 800 °C and at strain rates higher than about 1 s^{-1}, which is actually in the regime of flow instability as predicted by the criterion given by Eq 2. The mechanism occurring in the second domain is discussed in a following section along with the manifestations of flow instabilities. Regarding the instability regime, the coarse grained material exhibited a much wider area of flow instability in the α-β range than did the coarser grained material, but in the β range, the deformation was free from flow instabilities in the coarse grained material unlike in the coarser grained material.

The interpretation of the lower strain rate domain in the processing map for the coarse grained material (Fig. 4b) is similar to that described above and consists of two deformation mechanisms in the α-β and β regimes merging at the transus. The microstructural features of a coarse grained specimen deformed in the α-β range (900 °C and 0.001 s^{-1}) are shown in Fig. 5(b), which exhibits globularization very similar to that observed in the coarser grained material (Fig. 5a). The Arrhenius plot for the coarse grained material is shown in Fig. 6, which yields apparent activation energy values similar to those obtained on the coarser grained material. Thus, the domain of globularization and its characteristics are not significantly affected by changing the grain size from coarser to coarse as can be expected from the intragranular nature of the mechanism.

3.4 Prior β-Cracking Regime

Additional microstructural investigations have revealed that at temperatures below about 800 °C and strain rates lower than about 0.1 s^{-1}, cracking at the prior β boundaries has occurred and a majority of cracks are found at the bulge regions of the compression specimen. Figure 4(a) schematically shows the crocking regime as dotted lines on the processing map, and a typical microstructure is shown in Fig. 7(a), which corresponds to a coarser grained specimen deformed at 750 °C and 0.01 s^{-1}. These cracks occurred preferentially on boundaries which were near 45° orientation with respect to the compression axis and may be termed "shear" cracks. The mechanism of cracking was discussed in detail in an earlier publication.[10] The cracks nucleate at the soft β layer existing at the interface between the primary α layer and the colony sideplates of the prior β boundary and grow under a combined state of stress existing at the bulge region of the compression specimen. The limiting condition for mitigating the formation of cracks is the occurrence of dynamic recrystallization of the primary α at the prior β boundary, which is ensured at higher temperatures and lower strain rates.

The regime of prior β cracking for the coarse grained material is shown schematically in Fig. 4(b), and this regime is wider than that in the coarser grained material (Fig. 4a). Figure 7(b) shows typical microstructure of a coarse grained specimen deformed at 750 °C and 0.01 s^{-1}, and the features of cracking such as its origin and orientation with respect to the compression axis are similar to those of the coarser material. The wider regime in the map for the coarse grained material can be attributed to the increased probability of the prior β boundaries with the near 45° orientation,

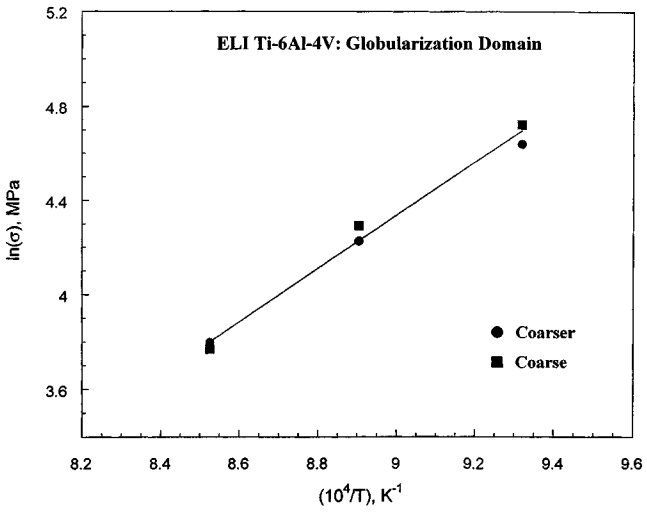

Fig. 6 Arrhenius plot showing the variation of the flow stress with the inverse of temperature in the globularization domain of Ti-6A1-4V

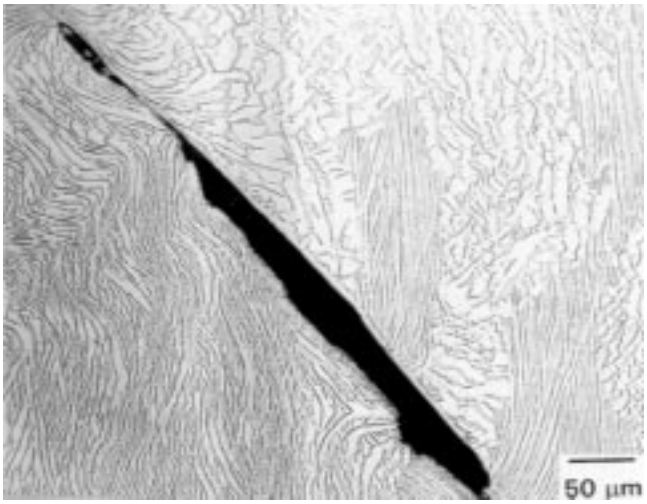

(a)

(b)

Fig. 7 Microstructures of Ti-6A1-4V specimens deformed at 800 °C and 0.01 s^{-1} exhibiting cracking at the prior β boundaries: **(a)** coarser grained material and **(b)** coarse grained material. The compression axis is vertical

which can help in enhancing the nucleation process. Thus, the results indicate that reducing the grain size from coarser to coarse grains is not beneficial from the point of view of prior β cracking because it restricts the globularization domain on the lower temperature side.

3.5 Mechanism of β-Deformation

The processing maps do not exhibit any specific domains in the β-deformation range because the power dissipation efficiencies are similar to those for the globularization domains. However, tensile ductility measurements in the β range have shown high elongations (≈100%) at a strain rate even as fast as 0.01 s^{-1}.[10] This suggests that mechanisms similar to those causing large grained superplasticity (LGSP) are responsible for the β deformation. The apparent activation energy for the process has been estimated using the kinetic rate equation.[3]

Figure 8 shows the Arrhenius plots using the data on the coarser and coarse grained materials in the β-temperature range. The plot yielded a value of about 256 kJ/mole, which is near that for self-diffusion in β titanium (153 kJ/mole),[12] suggesting that the process is controlled by diffusion. The prior β-grain size does not have much influence on the apparent activation energy. On the basis of high elongations, moderate strain rate sensitivity (≈0.3), the apparent activation energy values, and the steady-state stress-strain curves (Fig. 3), it can be concluded that LGSP is the most likely mechanism of β deformation. It is likely that the prior Widmanstätten colony boundaries within large β grains are stable during deformation and tend to slide under shear stress when their orientation is near 45° with respect to the compression axis. The sliding process contributes significantly to the total strain if the stress at their triple junctions is accommodated by diffusional flow, which is possible at higher temperatures (*e.g.*, 1050 °C). The characteristics of LGSP domain are not affected by the prior β-grain size as expected from the intragranular (within the β grains) nature of the mechanism as explained previously.

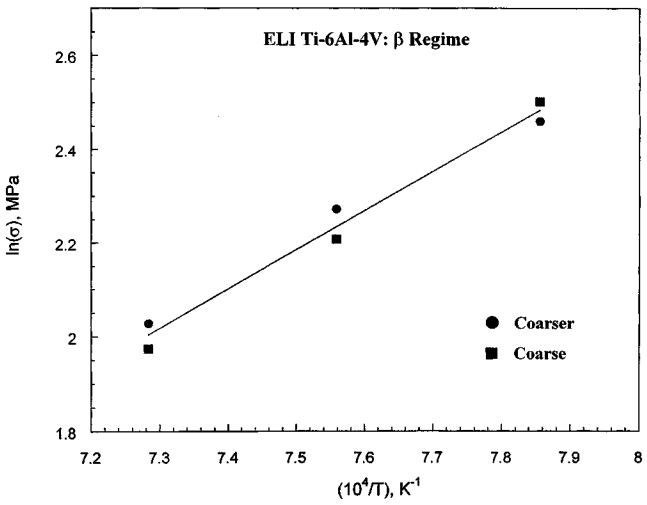

Fig. 8 Arrhenius plot showing the variation of the flow stress with the inverse of temperature in the β regime of Ti-6-4

3.6 Flow Instabilities

A comparison of the flow instability regimes in the processing maps for the coarse and coarser grained materials (Fig. 4a and b) reveals that the instability regime in the α-β range is wider in the coarse material than the coarser material, while that in the β regime occurs only in the coarser material. While the manifestation of the β instability is difficult to capture metallographically due to the phase transformation occurring during cooling of the specimen, the nature of the flow instabilities in the α-β regime can be studied in detail using microstructural observations.

Typical microstructures obtained on specimens deformed in the instability regime at 750 °C/100 s^{-1} and 850 °C/100 s^{-1} are shown in Fig. 9 and 10, respectively. In each of the figures, the micrographs for the coarser and coarse grained materials are compared. At 750 °C, intense adiabatic shear banding has occurred in both the materials, although the adiabatic shear bands resulted in cracking of the specimens in the coarse material (Fig. 9b), thereby showing a domain of high efficiency (Fig. 4b). The flow localization bands became increasingly diffused with increasing temperature (Fig. 9 vs Fig. 10). Figure 11 shows the microstructures recorded on specimens deformed at 850 °C/10 s^{-1}, and

(a)

(b)

Fig. 9 Microstructures obtained on Ti-6A1-4V specimens deformed at 750 °C and 100 s^{-1}: **(a)** coarser grained material and **(b)** coarse grained material. The compression axis is vertical

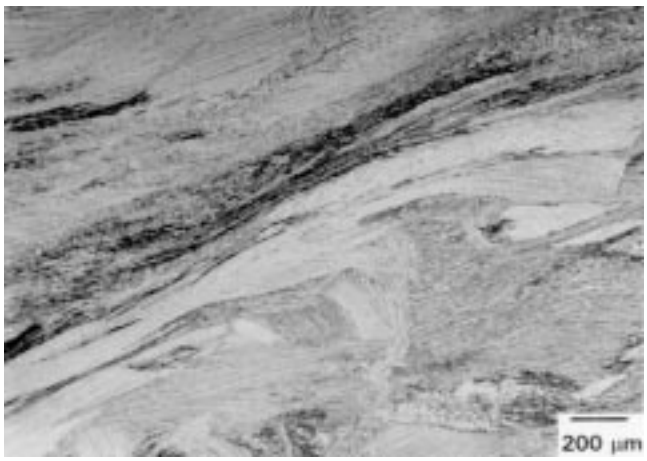

(a)

(b)

Fig. 10 Microstructures obtained on Ti-6A1-4V specimens deformed at 850 °C and 100 s^{-1}: **(a)** coarser grained material and **(b)** coarse grained material. The compression axis is vertical

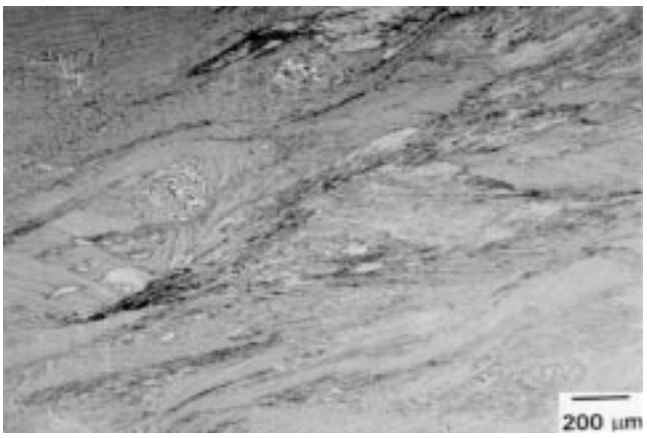

(a)

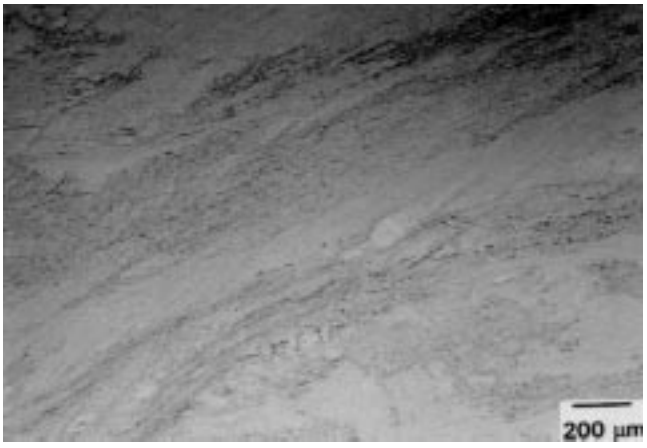

(b)

Fig. 11 Microstructures obtained on Ti-6A1-4V specimens deformed at 850 °C and 10 s^{-1}: **(a)** coarser grained material and **(b)** coarse grained material. The compression axis is vertical

a comparison with Fig. 10 reveals that the intensity of flow localization reduces with a decrease in strain rate.

The formation of the flow localization bands can be attributed to the adiabatic conditions created during deformation and the low thermal conductivity of Ti-6A1-4V. The heat generated at higher strain rates was not conducted away due to insufficient time, which reduces the flow stress locally leading to flow localization. In the case of coarser material, the higher temperature limit for flow instability is less by about 50 °C than that of the coarse material, and this difference can be attributed to the extent of flow softening observed in these two grain sizes (Fig. 2a and b). At strain rates higher than 1 s^{-1}, the coarse grained material has a much higher degree of flow softening than the coarser material.

Unlike the coarse grained material, the coarser material does not exhibit flow localization at temperatures higher than about 900 °C. A comparison of the microstructures of specimens deformed at 900 °C/100 s^{-1} is given in Fig. 12, which confirms the previous conclusion. Thus, the results on the instability analysis and microstructural validation show that the coarser grained material exhibits narrower regimes of flow instability in the α-β regime than does the coarse grained material. However, in the β-deformation range of coarser material, flow instabilities occur at strain rates higher than 10 s^{-1}.

4. Conclusions

The hot deformation behavior of ELI grade Ti-6A1-4V has been studied in coarse and coarser (prior β) grained specimens using processing maps in the temperature range 750 to 1100 °C and a strain rate range of 0.001 to 100 s^{-1}. The interpretations are validated by microstructural examination. The following conclusions can be drawn from this investigation on the influence of prior β-grain size.

- The process of globularization of the ($\alpha + \beta$) lamellae and the process of large grained superplasticity of the β phase are not significantly influenced by the prior β-grain size, because both the mechanisms are essentially intragranular in nature.
- The region of prior β-boundary cracking occurring at lower temperatures and strain rates is wider in the coarse grained material than the coarser material.

(a)

(b)

Fig. 12 Microstructures obtained on Ti-6A1-4V specimens deformed at 900 °C and 100 s^{-1}: **(a)** coarser grained material and **(b)** coarse grained material. The compression axis is vertical

- The flow instability regime in the α-β range, which manifests as adiabatic shear band formation and flow localization, is wider in the coarse grained material than in the coarser material. However, the flow instability of the β deformation is prominent in the coarser grained material.
- From the hot workability viewpoint, the present results show that there is no remarkable benefit in refining the prior β-grain size. Conversely, it will somewhat restrict the workability domain by widening the damage regimes.

Acknowledgments

One of the authors, Y.V.R.K. Prasad, is thankful to the National Research Council, United States, for awarding him an associateship and to the Director of the Indian Institute of Science, Bangalore, for granting him a sabbatical leave. The assistance rendered by Messrs. S. Sasidhara and R. Ravi of the Department of Metallurgy, Indian Institute of Science, is also gratefully acknowledged.

References

1. *Materials Properties Handbook: Titanium Alloys*, R. Boyer, G. Welsch, and E.W. Collings, eds., ASM International, Materials Park, OH, 1994, pp. 594-617.
2. M. Brun, N. Anoshkin, and G. Shakhanova: *Mater. Sci. Eng. A*, 1998, vol. 243, pp. 77-81.
3. S.L. Semiatin, V. Seetharaman, A.K. Ghosh, E.B. Shell, M.P. Simon, and P. Fagin: *Mater. Sci. Eng. A*, 1998, vol. 256, pp. 92-110.
4. H.G. Suzuki, H. Fujii, N. Takano, and K. Kaku: *6th World Conf. on Titanium*, P. Lacombe, R. Tricot, and G. Béranger, eds., Societé Francaise de Metallurgie, Les Ulie Cedex, France, 1988, pp. 1427-32.
5. Y.V.R.K. Prasad: *Ind. J. Technol.*, 1990, vol. 28, pp. 435-51.
6. Y.V.R.K. Prasad and T. Seshacharyulu: *Int. Mater. Rev.*, 1998, vol. 43 (1), pp. 243-58.
7. Y.V.R.K. Prasad and S. Sasidhara: *Hot Working Guide: A Compendium of Processing Maps*, ASM International, Materials Park, OH, 1997.
8. H. Ziegler: *in Progress in Solid Mechanics*, I.N. Sneddon and R. Hill, eds., North-Holland, Amsterdam, 1963, vol. 4., pp. 93-193.
9. H.L. Gegel, J.C. Malas, S.M. Doraivelu, and V.M. Shende: *Metals Handbook*, vol. 14, *Forging and Forming*, ASM International, Metals Park, OH, 1988, pp. 418.
10. T. Seshacharyulu, S.C. Medeiros, J.T. Morgan, J.C. Malas, W.G. Frazier, and Y.V.R.K. Prasad: *Mater. Sci. Eng. A*, 2000, vol. 279, pp. 289-99.
11. T. Seshacharyulu, S.C. Medeiros, J.T. Morgan, J.C. Malas, W.G. Frazier, and Y.V.R.K. Prasad: *Scripta Mater.*, 1999, vol. 41 (3), pp. 283-88.
12. N.E.W. de Reca and C.M. Libanati: *Acta Metall.*, 1968, vol. 16, pp. 1297-1305.